Silicon electro-optic modulators using p-i-n diodes embedded 10-micron-diameter microdisk resonators

Linjie Zhou and Andrew W. Poon

Photonic Device Laboratory, Department of Electronic and Computer Engineering, The Hong Kong University of Science and Technology, Clear Water Bay, Hong Kong SAR, China
eeawpoon@ust.hk

Abstract: We demonstrate a silicon electro-optic modulator using a 10-micron-diameter microdisk resonator with a laterally integrated p-i-n diode surrounding essentially the entire microdisk. Our experiments reveal a modulation bandwidth of 510 MHz using a Q ~ 16,900 resonance mode under a square-wave drive voltage of ~0.9 V forward bias and ~-6 V reverse bias.

OCIS codes: (060.4080) Modulation; (250.7360) Waveguide modulators; (250.5300) Photonic integrated circuits.

References and links

1. G. T. Reed and A. P. Knights, *Silicon Photonics*, (John Wiley, Chichester UK 2004).
2. L. Pavesi and D. J. Lockwood (Eds.), *Silicon Photonics*, (Springer-Verlag, Berlin, Germany 2004).
3. J. Niehusmann, A. Vörckel, P. H. Bolivar, T. Wahibrink, W. Henschel, and H. Kurz, "Ultrahigh-quality-factor silicon-on-insulator microring resonator," Opt. Lett. **29**, 2861-2863 (2004).
4. A. Vörckel, M. Mönster, W. Henschel, P. H. Bolivar, and H. Kurz, "Asymmetrically coupled silicon-on-insulator microring resonators for compact add-drop multiplexers," IEEE Photon. Technol. Lett. **15**, 921-923 (2003).
5. P. Dumon, W. Bogaerts, V. Wiaux, J. Wouters, S. Beckx, J. V. Campenhout, D. Taillaert, B. Luyssaert, P. Bienstman, D. V. Thourhout, and R. Baets, "Low-loss SOI photonic wires and ring resonators fabricated with deep UV lithography," IEEE Photon. Technol. Lett. **16**, 1328-1330 (2004).
6. I. Kiyat, A. Aydinli, and N. Dagli, "High-Q silicon-on-insulator optical rib waveguide racetrack resonators," Opt. Express **13**, 1900-1905 (2005).
7. W. R. Headley, G. T. Reed, S. Howe, A. Liu, and M. Paniccia, "Polarization-independent optical racetrack resonators using rib waveguides on silicon-on-insulator," Appl. Phys. Lett. **85**, 5523-5525 (2004).
8. D. Xu, S. Janz, and P. Cheben, "Design of polarization-insensitive ring resonators in silicon-on-insulator using MMI couplers and cladding stress engineering," IEEE Photon. Technol. Lett. **18**, 343-345 (2006).
9. D. K. Sparacin, C. Hong, L. C. Kimerling, J. Michel, J. P. Lock, and K. K Gleason, "Trimming of microring resonators by photo-oxidation of a plasma-polymerized organosilane cladding material," Opt. Lett. **30**, 2251-2253 (2005).
10. M. Borselli, T. J. Johnson, and O. Painter, "Beyond the Rayleigh scattering limit in high-Q silicon microdisks: theory and experiment," Opt. Express **13,** 1515-1530 (2005).
11. T. Indukuri, P. Koonath, and B. Jalali, "Subterranean silicon photonics: demonstration of buried waveguide-coupled microresonators," Appl. Phys. Lett. **87**, 081114 (2005).
12. A. Kazmierczak, M. Brière, E. Drouard, P. Bontoux, P. Rojo-Romeo, I. O'Connor, X. Letartre, F. Gaffiot, R. Orobtchouk, and T. Benyattou, "Design, simulation, and characterization of a passive optical add-drop filter in silicon-on-insulator technology," IEEE Photon. Technol. Lett. **17**, 1447-1449 (2005).
13. C. Y. Chao and L. J. Guo, "Design and optimization of microring resonators in biochemical sensing applications," J. Lightwave Technol. **24**, 1395-1402 (2006).
14. G. N. Nielson, D. Seneviratne, F. Lopez-Royo, P. T. Rakich, Y. Avrahami, M. R. Watts, H. A. Haus, H. L. Tuller, and G. Barbastathis, "Integrated wavelength-selective optical MEMS switching using ring resonator filters," IEEE Photon. Technol. Lett. **17**, 1190-1192 (2005).
15. M. M. Lee and M. C. Wu, "MEMS-actuated microdisk resonators with variable power coupling ratios," IEEE Photon. Technol. Lett. **17**, 1034-1036 (2005).
16. S. Yamagata, T. Kato and Y. Kokobun, "Non-blocking wavelength channel switch using TO effect of double series-coupled microring resonator," Electron. Lett. **41**, 593-595 (2005).
17. I. Kiyat, A. Aydinli, and N. Dagli, "Low-power thermooptical tuning of SOI resonator switch," IEEE Photon. Technol. Lett. **18**, 364-366 (2006).

#71904 - $15.00 USD Received 12 June 2006; revised 17 July 2006; accepted 18 July 2006

18. R. A. Soref and B. R. Bennett, "Electrooptical effects in silicon", IEEE J. Quant. Electron. **23**, 123-129 (1987).
19. Q. Xu, B. Schmidt, S. Pradhan, and M. Lipson, "Micrometer-scale silicon electro-optic modulator," Nature **435**, 325-327 (2005).
20. C. Manolatou and M. Lipson, "All-optical silicon modulators based on carrier injection by two-photon absorption," J. Lightwave Technol. **24**, 1433-1439 (2006).
21. L. Zhou and A. W. Poon, "Silicon-on-insulator tunable waveguide-coupled microdisk resonators with selectively integrated p-i-n diodes," in *Proceedings of Conference on Lasers Electro-Optics*, Baltimore, MD (Optical Society of America, Washington, D. C., 2005).
22. V. R. Almeida, R. R. Panepucci, and M. Lipson, "Nanotaper for compact mode conversion," Opt. Lett. **28**, 1302-1305 (2003).

1. Introduction

Silicon photonics have attracted considerable research interest in recent years, largely stimulated by their compatibility with mature silicon microelectronics fabrication processes and the holy grail of high-density integration of compact photonic devices and electronics on a single chip [1, 2]. Among various micro- and nano-photonics technologies, microring and microdisk resonators have long been regarded as possible building blocks for large-scale-integrated photonic circuits, due to their micrometer-scale size and high-Q resonances. Microring and microdisk resonator-based passive devices have been demonstrated by many research groups as wavelength-division-multiplexing filters [3-12] and also for biochemical sensing applications [13]. In order to actively switch silicon microring and microdisk resonators, various mechanisms have been investigated including microelectromechanical system (MEMS) [14, 15], thermo-optic effect [16, 17], free-carrier plasma dispersion effect [18, 19], and all-optical tuning using photo-excited free carriers and two-photon absorption [20]. Most notably, Xu *et al*. [19] demonstrated the first micrometer-scale silicon electro-optic modulator using a microring resonator with laterally integrated p-i-n diodes. The microring high-Q resonance, with the plasma-dispersion induced resonance wavelength shifts, enables the transmission optical signal rise time to be significantly shorter than the free-carrier injection time.

Here we report an alternative design to realize microresonator-based silicon electro-optic modulators by using a p-i-n diode integrated microdisk resonator. Microdisk resonators are distinct from microring resonators. Microdisk resonators have the key merit of having only one outer sidewall, and thus the sidewall roughness induced scattering losses is relatively small (potentially giving high-Q resonances) compared with microring resonators that suffer from both the outer and inner sidewall scattering losses. Furthermore, the microdisk resonator modes are whispering-gallery modes (WGMs), with light wave localized near the microdisk rim and grazing along the circumference. The device implication is that we can actively switch the resonance modes propagating in the vicinity of the microdisk rim, by means of injecting free carriers into the optical modes from an embedded p-i-n diode structure that has the lossy heavily-doped regions only in the microdisk central region and outside the microdisk rim.

2. Device design

Figure 1 shows the three-dimensional schematic of our p-i-n diode integrated microdisk resonator-based electro-optic modulator on a silicon-on-insulator (SOI) substrate. The modulator comprises a 10-μm-diameter p-i-n diode embedded microdisk resonator laterally coupled to a 0.35-μm-wide straight single-mode waveguide. The gap separation between the waveguide and the microdisk sidewall is 0.35 μm. We remark that the waveguide width and the relatively large gap separation design are limited by our photolithography resolution of ~0.35 μm. The waveguide and microdisk resonator is 0.21 μm high and etched depth is 0.18 μm.

#71904 - $15.00 USD Received 12 June 2006; revised 17 July 2006; accepted 18 July 2006

We embed a heavily-doped n^+-type region in the microdisk central region with a radius of 3.25 μm and a heavily-doped 3-μm-wide p^+-type region in the slab layer outside the microdisk (with a 0.5 μm separation from the microdisk sidewall). This constitutes the lateral p-i-n diode with the microdisk rim as the intrinsic region. As the WGMs are partially confined and localized in the vicinity of the microdisk rim intrinsic region, free-carrier absorption and scattering losses due to the n^+ and p^+ doped regions are minimized and can be engineered (e.g., by varying the central doped region radius and the separation between the microdisk sidewall and the doped region in the slab layer). Moreover, as high-order WGMs field extend into the microdisk bulk, it is possible to suppress high-order modes by means of the excessive losses in the doped central region [21].

We position a 2-μm-wide trench outside the p^+-doped region in the slab layer in order to confine the current flow and also to isolate the microdisk modulator from other integrated devices. It is noteworthy that the doped region in the slab layer and the trench surround almost the entire microdisk, only leaving enough room (0.5 μm from the waveguide sidewalls) for the coupled waveguide to pass through. The separate p^+-doped regions at the two sides of the waveguide are electrically connected by metal wires, and thus free-carriers can be injected into and swept out from waveguide-resonator coupling region simultaneously with those in the microdisk rim. This potentially reduces the free-carriers lateral diffusion times, as first suggested by Q. Xu *et al* [19].

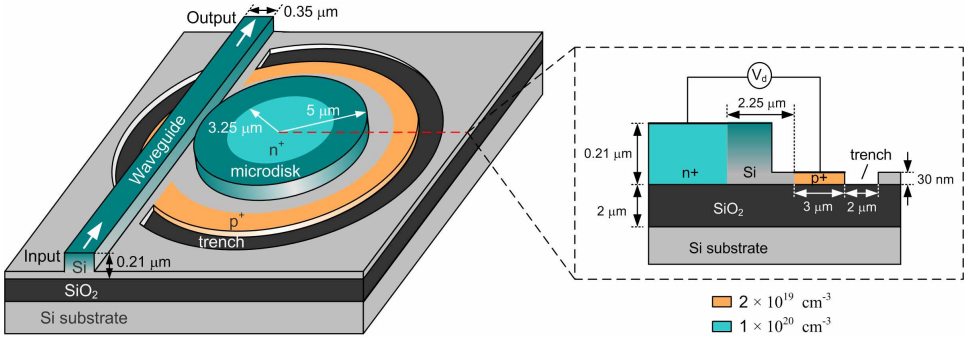

Fig. 1. Schematic of a silicon 10-μm-diameter microdisk resonator-based modulator using a laterally embedded p-i-n diode. The p-i-n diode and a 2-μm-wide trench surround almost the entire microdisk except in the vicinity of the coupled waveguide. Inset: cross-sectional view of the lateral p-i-n diode. The n^+-doped region radius is 3.25 μm. The p^+-doped region width is 3 μm. The p-i-n diode intrinsic region width is 2.25 μm.

The inset shows the schematic cross-section of our lateral p-i-n diode (along the red dashed line). The p-i-n diode intrinsic region width is 2.25 μm (between the n^+-doped region edge and the p^+-doped region edge). Here we minimize the intrinsic width in order to reduce the carrier transit time inside the p-i-n diode, yet not inducing excess scattering and absorption losses from the n^+ and p^+-doped regions. Upon forward bias, free-carriers are injected into the microdisk rim and spatially overlap with the WGM field, resulting in resonance tuning and intensity modulation at a probe wavelength near the resonance wavelength.

3. Device fabrication

We use 0.55-μm SOI wafers with 2-μm buried oxide (BOX) layers for the device fabrication. In order to get a desired 0.21-μm-thick device layer, we use wet oxidation to thin down the top silicon layer. Half of the oxidized layer is removed using buffered oxide etchant (BOE) solution and the other half (~0.38 μm) is left as a hard mask for dry etching. We employ i-line (365 nm) photolithography to define the device patterns and CF_4-based reactive ion etching (RIE) to transfer the patterns onto the silicon device layer. We implant phosphorous

#71904 - $15.00 USD Received 12 June 2006; revised 17 July 2006; accepted 18 July 2006

(concentration of 1×10^{20} cm^{-3}) and boron (2×10^{19} cm^{-3}) dopants to form the n^+ and p^+-doped regions. An upper cladding of 0.6-μm-thick low temperature oxide (LTO) is deposited as an electrical isolation layer. Lastly, a 0.7-μm-thick aluminum is sputtered and patterned for electrical connection.

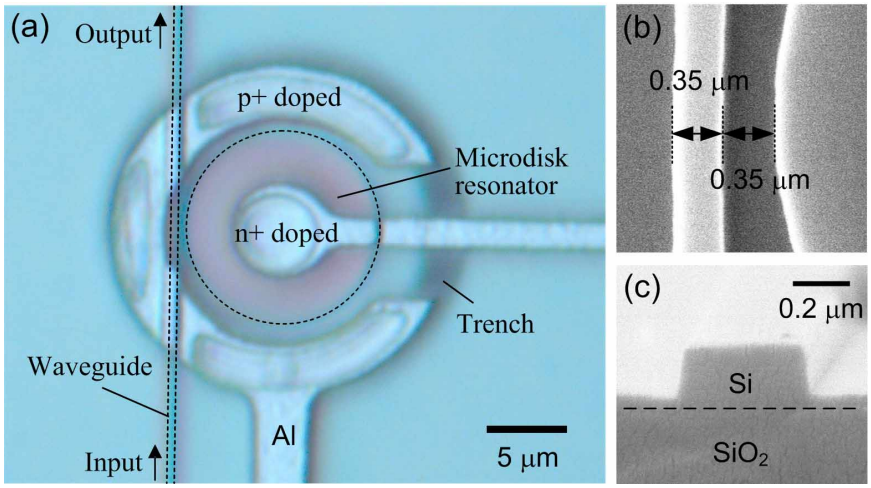

Fig. 2. (a) Optical micrograph of our fabricated p-i-n diode integrated microdisk modulator. (b) Scanning electron micrograph (SEM) of the waveguide-microresonator coupling region. The waveguide width is ~0.35 μm and the gap size is ~0.35 μm. (c) Cross-sectional view SEM of the single-mode waveguide.

Figure 2(a) shows the top-view optical micrograph of our fabricated 10-μm-diameter microdisk modulator. The dashed lines highlight the straight waveguide and the microdisk resonator, which are underneath the oxide upper cladding layer. Aluminum wires are connected to the p-i-n diode doped regions. The dark shadow shows the circular trench underneath.

Figure 2(b) shows the zoom-in scanning electron micrograph (SEM) of the waveguide-microresonator coupling region before the LTO deposition. The fabricated waveguide width and gap separation are ~0.35 μm. The microdisk sidewall, however, displays multiple facets due to the photomask resolution. Figure 2(c) shows the cross-sectional view SEM of the single-mode waveguide, showing reasonably vertical sidewalls and the deeply-etch rib waveguide profile.

4. Device characterization

We measure the microdisk resonator spectra and the transmission intensity modulation by using an external-cavity wavelength-tunable diode laser (1510 nm -1580 nm, ~300 kHz linewidth). Laser light from a tapered-lensed polarization-maintaining singlemode fiber in the TE polarization (electric field parallel to the chip) is end-fired into the input-coupled waveguide. The waveguide end-face is laterally tapered to ~2 μm. The waveguide throughput and drop-port intensities are separately imaged by an objective lens (N.A. = 0.65) through a TE-polarization analyzer. For spectral measurements, the imaged intensities are lock-in detected with a photodiode.

For active modulation measurements, the imaged intensities are first amplified by using an Erbium Doped Fiber Amplifier (EDFA) with a gain of ~20 dB and selected by a band-pass filter (linewidth ~ 5 nm) before recorded by a 1-GHz-bandwidth photodetector. The resulting electrical signals are measured by a 20-GHz-bandwidth oscilloscope. We use a 3.6-GHz-bandwidth transmission analyzer to generate the electrical driving signals and a 3.5-GHz-bandwidth RF probe to apply them onto the device.

#71904 - $15.00 USD Received 12 June 2006; revised 17 July 2006; accepted 18 July 2006

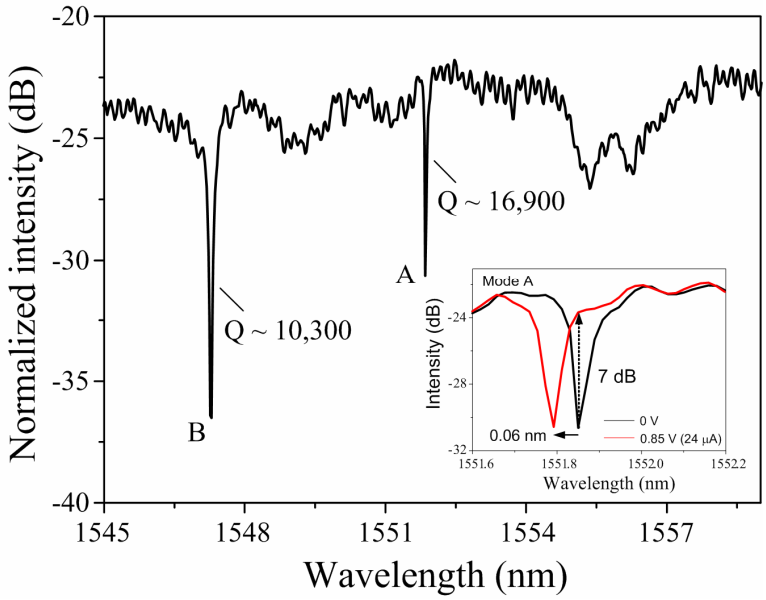

Fig. 3. Measured TE-polarized throughput-port spectrum of the microdisk resonator without biasing the p-i-n diode. Inset shows the DC tuning of resonance mode A. Resonance wavelength blueshifts by ~0.06 nm upon a 0.85 V forward bias across the p-i-n diode.

Figure 3 shows the typical measured TE-polarized throughput-port spectrum of the microdisk modulator without biasing the p-i-n diode. We discern two main resonance modes, donated as modes A and B. Mode A has a high Q value of ~16,900 and an extinction ratio of ~7 dB. Mode B has a low Q value of ~10,300 and an extinction ratio of ~12 dB. We remark that our device insertion loss of ~23 dB (relative to the input fiber transmitted intensity) is relatively high. We attribute the insertion loss partially to high input end-face reflection (~1.5 dB) and mode-mismatch losses (~12 dB) and partially to high waveguide propagation loss (estimated ~20 dB/cm by cut back method). The input coupling losses can be mitigated by improved coupling techniques such as coating the input end facet with an antireflection layer and using an inverted taper [22]. The waveguide propagation loss mainly comes from sidewall roughness (due to photolithography and dry etching) and substrate leakage, which can be improved using e-beam lithography and an optimized waveguide profile with a thicker under-cladding layer.

The inset shows the measured resonance mode A wavelength blueshift of ~0.06 nm upon applying a DC forward bias of 0.85 V. It is notable that such small blueshift is sufficient to result in a 7 dB transmission intensity increment at a probe wavelength at the passive resonance wavelength. We estimate the diode current to be ~24 μA (based on an I-V measurement), inducing an estimated ~6.8×10^{16} cm^{-3} free carriers (electrons and holes) concentration increment in the intrinsic region. Our simulations based on MEDICI semiconductor simulator also suggest a uniform carrier distribution in the intrinsic region upon a DC 0.85-V forward bias. Using the free-carrier plasma dispersion relation by Soref and Bennet [18], we estimate a refractive index change Δn of about -3×10^{-4} and an absorption coefficient change $\Delta\alpha$ of about 1 cm^{-1} in the intrinsic region. However, the observed ~0.06 nm blueshift suggests a Δn of only about -1.35×10^{-4}. We attribute the discrepancy to the accompanied thermo-optic effect that can possibly raise the refractive index by $\sim2 \times 10^{-4}$ upon a temperature increment of ~1 ^{o}C under the ~20 μW electrical power dissipation.

#71904 - $15.00 USD Received 12 June 2006; revised 17 July 2006; accepted 18 July 2006

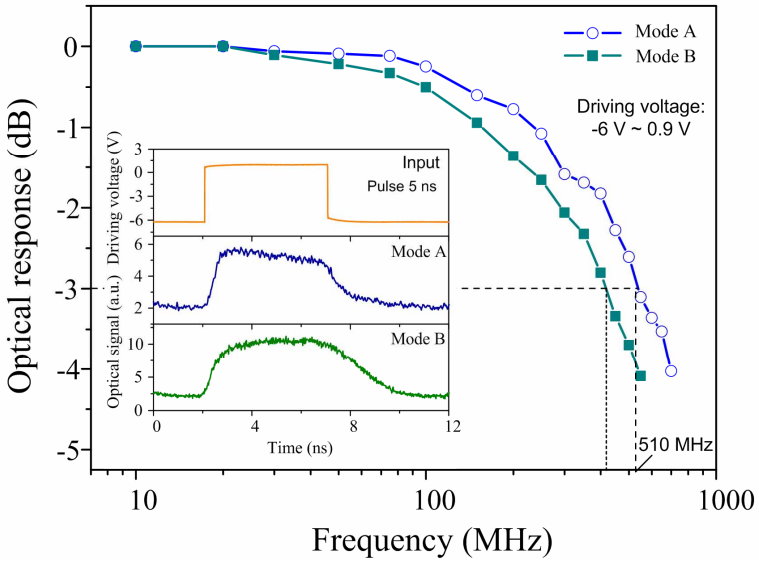

Fig. 4. Measured modulation bandwidths for mode A (open circles) and mode B (solid squares). The driving electrical signal is 0.9 V forward bias and -6.0 V reverse bias. Inset: optical transient responses to a 5-ns input electrical pulse for modes A and B. Mode A: τ_{rise} ~ 417 ps and τ_{fall} ~1.1 ns, mode B: τ_{rise} ~ 850 ps and τ_{fall} ~2.1 ns.

We apply a square-wave radio-frequency (RF) drive signal with a forward bias of 0.9 V and a reverse bias of -6 V in order to characterize the microresonator electro-optic modulation responses. The reverse bias is essential in order to sweep out the injected carriers for fast modulation. We set the probe wavelengths near modes A and B, and measure the optimal modulation depth as a function of electrical signal frequency. Figure 4 shows the measured normalized modulation depth (relative to low-frequency modulation depth) varies with modulation frequency for modes A (open circles) and B (solid squares). For mode A, we measure the low-frequency modulation depth to be ~7 dB, and the 3-dB modulation bandwidth to be ~510 MHz. For mode B, we measure the low-frequency modulation depth to be ~12 dB, and the 3-dB modulation bandwidth to be ~410 MHz.

At low frequencies, the free carrier concentrations in the intrinsic region essentially follow the applied electrical signal, and thus the resonance wavelength can be fully blueshifted during the diode on-cycles and shifted back to the resonance wavelength during the diode off-cycles. This results in an optical waveform with the optimum modulation depth at a probe wavelength near the resonance. As the signal period becomes comparable to the carriers transit times (estimated ~few ns), the carrier injection into and extraction from the p-i-n diode intrinsic region (the microdisk rim) cannot totally follow the drive signal, resulting in a narrowed dynamic range for the resonance wavelength shifts. The resonance profiles of the diode off and on-cycle thus approach each other, leading to a reduced modulation depth. As the higher-Q resonance mode is more sensitive to small changes in refractive index, the transmission intensity responds to smaller carrier concentration changes, and thus enables a higher 3-dB modulation bandwidth.

The inset of Fig. 4 shows the measured optical waveforms upon a 5-ns electrical square pulse for modes A and B. We measure an optical rise time τ_{rise} of 417 ps for mode A and 850 ps for mode B, yet we measure a relatively long optical fall time τ_{fall} of 1.1 ns for mode A and 2.1 ns for mode B. We remark that the -6 V reverse bias has significantly reduced the fall times (from ~5 ns with -1 V reverse bias for mode A). Yet further increases in the reverse

#71904 - $15.00 USD Received 12 June 2006; revised 17 July 2006; accepted 18 July 2006

bias voltage shows no significant reduction in the fall times. Thus, our injection-type modulator speed is limited by the ns-range fall times.

Considering our p-i-n diode vertical profile (Fig. 1 inset), we speculate that the step-like vertically asymmetric diode architecture (with 210-nm-thick n^+-doped region and only 30-nm-thick p^+-doped region) may render the RF electromagnetic field distribution to be non-uniform in the microdisk intrinsic rim region, and with possibly weaker field amplitudes nearby the microdisk upper edge. This may impose a limit to the effectiveness of the free-carrier extraction upon the ns-duration reverse bias and leave the residual free carriers to slowly recombine at the microdisk surfaces.

5. Conclusion

In conclusion, we have demonstrated a 10-μm-diameter silicon microdisk resonator-based electro-optic modulator with a laterally integrated p-i-n diode. To our knowledge, this is the smallest microdisk-based silicon electro-optic modulator. In order to enable fast free carriers sweep out and to enhance the electrical confinement, we surround essentially the entire microdisk with the lateral p-i-n diode and an isolation trench. The measured modulation bandwidths are 510 MHz for a Q ~ 16,900 resonance mode and 410 MHz for a Q ~ 10,300 mode, using a 0.9 V forward bias and a -6 V reverse bias electrical signal. Optical transient response measurements revealed that our device modulation speed is primarily limited by slow fall times (~1 ns - ~2 ns).

Acknowledgement

The research was substantially supported by a grant from the Research Grants Council of the Hong Kong Special Administrative Region, China (Project No. 618505). We also acknowledge the support by a grant from the Institute of Integrated Micro Systems (Project No. I2MS01/02.EG07).

#71904 - $15.00 USD Received 12 June 2006; revised 17 July 2006; accepted 18 July 2006